International Journal of Concrete Structures and Materials

RESEARCH

Open Access

Hybrid Reinforced Concrete Cross-Section Using Fiber-Reinforced Polymer and Steel Bars

Zahid Hussain[1*], Federico Tuozzo[2], Gennaro Magliulo[2] and Antonio Nanni[1]

Abstract

Fiber-reinforced polymer (FRP) bars offer a promising alternative to conventional steel reinforcement in reinforced concrete (RC) structures, primarily due to their corrosion resistance. However, their intrinsic linear elastic behavior may limit their applications to non-seismic zones or regions with limited seismic activity. To extend their applications in seismic zones such as Seismic Design Category D, a novel approach involving a hybrid-RC (HRC) cross-section is proposed. This approach entails placing FRP bars on the cross-section exterior for corrosion resistance, while steel bars on the inner side of the cross-section to ensure ductility and energy dissipation. This paper presents a methodology for designing HRC cross-sections and evaluates their ductility and energy dissipation capabilities. The discussion encompasses various design aspects of an HRC section including strength reduction factor, minimum reinforcement ratio, reinforcement strain, concrete shear strength, and the impact of confinement on ductility and energy dissipation. Additionally, an illustrative example of a HRC section demonstrates the practicality of the proposed design methodology in practical applications.

Keywords Hybrid reinforcement, FRP bars, Steel bars, Ductility, Energy dissipation

1 Introduction

The corrosion of steel reinforcement within concrete structures has emerged as a significant factor contributing to the degradation of the reinforced concrete (RC) built stock. This deterioration often leads to a reduction in the useful service life of the structures, accompanied by increased costs associated with repairs and strengthening. Fiber-reinforced polymer (FRP) bars have emerged as a promising alternative to traditional steel reinforcement in concrete structures to mitigate the above challenges. However, their inherently brittle nature has limited their widespread adoption, particularly in seismic regions. The linear elastic behavior of FRP bars presents a challenge in defining their ductility index. Structures reinforced with glass-FRP (GFRP) exhibit brittle failure characteristics without the formation of plastic hinges, thereby offering minimal energy dissipation. The lack of energy dissipation has been a significant barrier to extending the use of GFRP in seismic zones. As per current practice, the use of GFRP bars is restricted to seismic zone with comparatively lower seismic activity (i.e., seismic design category (SDC) A) (ACI Committee440, 2022).

The evaluation of ductility and its crucial role in structural design cannot be overstated. Ductility serves as a vital characteristic, allowing structures to withstand exceptional actions such as earthquakes by providing a reserve of deformation beyond the elastic phase. This ability to undergo controlled yielding and deformation enables structures to dissipate energy, mitigating the effects of dynamic loads and averting catastrophic failure. Understanding the constitutive behavior of materials under various loading conditions is essential for assessing

Journal information: ISSN 1976-0485 / eISSN 2234-1315.

*Correspondence:
Zahid Hussain
zxh446@miami.edu
[1] Department of Civil and Architectural Engineering, University of Miami, Coral Gables, FL 33146, USA
[2] Department of Structures for Engineering and Architecture, University of Naples Federico II, Via Claudio 21, 80125 Naples, Italy

ductility. At the section level, ductility is often quantified through the moment–curvature diagram, representing the section's capacity for further deformation beyond the elastic range.

GFRP-RC cross-sections offer considerable deformability capacities; however, they do not provide energy dissipation due to GFRP brittle nature. The concept of hybrid reinforcement, combining GFRP and steel bars, presents a novel approach to address challenges related to ductility and energy dissipation in GFRP-RC structures. Strategically placing steel bars at a distance of 75 mm from the cross-section surface for protection against corrosion, and GFRP bars at a distance of 38 mm from the surface for fire protection will enable both durability and energy dissipation. Consequently, this study addresses concrete cross-sections designed incorporating hybrid reinforcement to provide insights into their design methodology, ductility, and energy dissipation capabilities.

2 Assumptions and Methodology

2.1 Effect of Stirrup's Confinement on Concrete Compressive Strength

Research has indicated that the presence of transverse reinforcement (i.e., stirrups, ties and spirals) in concrete enhances its compressive strength. This augmentation in strength brings a significant improvement in ductility and energy dissipation. Notably, Euro and Italian codes incorporate provisions to differentiate between unconfined and confined concrete cross-sections, focusing on confinement provided by steel stirrups (Comité Européem de Normalisation, 2004; NTC, 2018, 2018). However, these codes do not directly account for the confinement effects stemming from GFRP transverse reinforcement. Well-confined GFRP-RC columns have shown an increase in strength and drift capacities (Prajapati et al., 2023). It is also reported that GFRP-RC columns achieved drift ratios of about 4-5% meeting seismic drift limitation of most building codes (Deng et al., 2018). GFRP-RC columns with stable post-peak response and high levels of deformability can be used to achieve desired levels of ductility (Tavassoli et al., 2015). An experimental study was conducted to investigate the confinement effect on the concrete compressive strength provided by three types of stirrups: steel, GFRP bar, and GFRP plate stirrups (Chen et al., 2018). Due to the shape of GFRP plate stirrups, these specimens achieved maximum strain at failure. The specimens with GFRP bar stirrups failed by the opening of stirrup legs; however, showed similar strain at failure as steel-RC. Hence, it can be inferred that GFRP stirrups provide similar confinement as that of steel stirrups. This assumption may be at first counterintuitive because GFRP stirrups have lower strength at the bends. This fact is addressed by specifications defining the strength of the bend as 60% of the strength of the straight bar (ACI Committee440, 2022; ASTM D7957/D7957M-22, 2022). Even with this reduction, GFRP stirrups offer comparable confinement as that of steel stirrups.

2.2 Minimum Reinforcement Area and Strength Reduction Factor

In the design of RC structures, a minimum amount of reinforcement is specified by design codes. The provision of minimum reinforcement area is to prevent failure of RC members upon the onset of concrete cracking and is defined as $\Phi M_n \geq 2M_{cr}$ for designing tension-controlled sections. Where, Φ, is strength reduction factor, M_n, is nominal moment capacity and M_{cr}, is the cracking moment. The requirements of minimum reinforcement in ACI 318-19 are based on this concept. These requirements for steel-RC were developed as follows.

The cracking moment of concrete cross-section can be calculated using the properties of concrete and cross-section dimensions as follows:

$$M_{cr} = \frac{f_r I_g}{y_t}. \tag{1}$$

f_r is the modulus of rupture of concrete given in ACI 440.11 and ACI 318-19 in section 19.2.3.1 as provided below in Eq. (2):

$$f_r = 0.62\sqrt{f_c'}, \tag{2}$$

whereas y_t is the distance from center of gravity of the cross-section to extreme compression or tension fiber. For an uncracked section, it is reasonable to take it equal to $h/2$, where h is the total depth of the section. The capacity of the cross-section may be calculated by multiplying tension or compression force with the moment arm as provided below:

$$M_n = A_s f_y \left(d - \frac{a}{2}\right), \tag{3}$$

where M_n, is the nominal capacity of the cross-section, A_s, is the area of tension reinforcement, d, is the effective depth (distance from extreme compression fiber to the center of the tensile reinforcement), f_y is the yield strength of steel and a is the depth of compression block. The depth of compression block will depend upon neutral axis depth.

Equating Eqs. (1) and (3) and multiplying right side by a factor 2 will provide a relationship for minimum

reinforcement area required to have an ultimate capacity two times greater than the cracking moment:

$$A_s f_y \left(d - \frac{a}{2}\right) = 2\frac{0.62\sqrt{f_c'} I_g}{y_t}.$$

Assuming the moment arm is approximately equal to $0.9d$, y_t equal to $h/2$, a rectangular cross-section with a moment of inertia equal to $bh^3/12$ and further simplification would result in a relation for minimum reinforcement to have a capacity twice the cracking moment of cross-section:

$$0.9dA_s f_y = 2\frac{0.62\sqrt{f_c'}\frac{bh^3}{12}}{\frac{h}{2}}$$

Finally, conservatively rounding off the digits would result in the following relationship for minimum reinforcement area provided in Eq. (4):

$$A_s = \frac{0.25\sqrt{f_c'}}{f_y} bd. \tag{4}$$

The relationship provided in Eq. (4), is the minimum reinforcement for a steel-RC cross-section. ACI Committee 440 extended the above equations for GFRP-RC members, where modifications resulted from different strength reduction factors. Because FRP members do not exhibit ductile behavior, a conservative strength reduction factor was adopted to provide a higher reserve of strength in the members. The Japanese recommendations for design of flexural members using FRP suggests a strength reduction factor equal to 0.77 (Japan Society of Civil Engineers, 1997). Other researchers suggest a value equal to 0.75 based on probabilistic concepts (Benmokrane & Masmoudi, 1995). Based on ACI 318, the Φ for design of a compression-controlled section for steel-RC is 0.65, with a target reliability index between 3.4 and 4.0. A reliability analysis on FRP-reinforced beams in flexure using Load combination 2 from ACI 318 for live-to-dead load ratios between 1 and 3 indicated reliability indexes between 3.5 and 4.0 when Φ was set to 0.65 for a compression-controlled section, and 0.55 for a tension-controlled section. Therefore, strength reduction factor equals to 0.65 and 0.55 for compression and tension-controlled FRP sections were, respectively, adopted in ACI 440.11 code (ACI 440.1R-15, 2015; ACI Committee440, 2022).

Utilizing difference in strength reduction factors between steel and GFRP, a minimum reinforcement area for GFRP-RC was proposed. The minimum reinforcement area for GFRP-reinforced members is obtained by multiplying the existing ACI 318 equation (i.e., Eq. (4) for steel-RC by 1.64 (i.e., 1.64 = 0.9/0.55). Note: for compression-controlled section minimum reinforcement requirement would be automatically satisfied. The minimum reinforcement requirements for a GFRP-RC are provided in ACI 440.11 as given below:

$$A_{fmin} = \frac{0.41\sqrt{f_c'}}{f_{fu}} bd, \tag{5}$$

where f_{fu} is the design tensile strength of GFRP longitudinal reinforcement.

The novel concept of hybrid-RC sections, however, offers both ductility and energy dissipation as required for a targeted seismic zone. Therefore, the strength reduction factor equals to 0.9 as in the case of steel-RC for tension-controlled section would be more reasonable. If a strength reduction factor equals to 0.9 instead of 0.55 is adopted, the minimum reinforcement area provided in Eq. (4) will govern. Therefore, for hybrid-RC cross-sections it is assumed that the minimum reinforcement area as provided in ACI 318-19 governs.

2.3 Strain Limit for Steel Reinforcement

Balanced reinforcement ratio provides a boundary between tension and compression-controlled sections. The strength reduction factors are then accordingly selected in the design of RC members. Considering failure of a hybrid-RC section at yielding of steel reinforcement, it is assumed that balanced reinforcement ratio resulting from force equilibrium in a steel-RC section would remain a reasonable assumption. The equation for calculating balanced reinforcement ratio used for steel-RC section is provided below:

$$\rho_b = \frac{0.85\beta_1 f_c'}{f_y}\left(\frac{\varepsilon_{cu}}{\varepsilon_{cu} + \varepsilon_y}\right), \tag{6}$$

where β_1 is factor relating depth of equivalent rectangular compressive stress block to depth of neutral axis, ε_{cu} is ultimate concrete deformation at extreme concrete compression fiber and ε_y the deformation of the steel at yield strength.

At failure, strain in steel reinforcement for a hybrid-RC section should be equal to or greater than 0.005. A strain value of 0.005 or greater in steel bars not only ensures the tension-controlled section but guarantees ductility and energy dissipation as well. Equally important, in order to avoid brittle failure, strain at failure in the GFRP reinforcement on tension face of the hybrid-RC section must always be lower than its ultimate value.

2.4 Shear Strength Contribution of Concrete and Stirrups

In the design of a hybrid-RC section, it was assumed that flexural capacity is provided by the combination of

GFRP, and steel reinforcement provided in different layers. However, the contribution of steel stirrups to shear in hybrid-RC section is still to be known. The steel stirrups lie in the core of the cross-section, hence traditional truss model for shear may not be applicable. In reality the shear strength in a hybrid-RC section should be combination of strength provided by concrete, GFRP shear stirrups, and steel stirrups. However, depending on size of cross-section and location of steel stirrups, the contribution of steel stirrups would change. The contribution of steel stirrups may be added to calculate shear strength as evidence of its magnitude becomes available in the future. Therefore, it is reasonably conservative to assume that only GFRP stirrups contribute to the shear strength of hybrid-RC section.

The total shear strength would then be combination of strength provided by concrete cross-section and GFRP stirrups as shown below:

$$V_n = V_c + V_f, \tag{7}$$

where V_n = nominal shear strength, kN; V_c = nominal shear strength provided by the concrete, kN; and V_f = nominal shear strength provided by GFRP shear reinforcement, kN.

It has been established that the shear capacity of members reinforced with GFRP bars would be different than those reinforced with steel reinforcement due to the different physio-mechanical properties of the two materials (Tureyen et al., 2003). ACI-ASCE Committee 445 has recognized that a cross-section's shear capacity depends on the longitudinal reinforcement's axial stiffness (Joint ACI-ASCE Committee445, 1998). Owing to the lower axial stiffness of GFRP bars (i.e., about one quarter), the flexural cracks will penetrate deeper into the GFRP-RC cross-section, and wider cracks would form, compared to steel-RC sections, even when more longitudinal reinforcement area is used. The formation of deeper flexural cracks decreases the depth of the uncracked concrete compression zone; thereby, the contribution of the cross-section to shear strength is reduced. Other than shear transmitted across the concrete compression zone, the shear capacity in steel-RC members is affected by aggregate interlock and dowel action. Given the wider crack widths, the aggregate interlock is less in the GFRP-RC cracked cross-section. Also, the dowel action in RC members is a function of the shear modulus of longitudinal reinforcing bars, controlled by resin in GFRP reinforcement. The smaller value of the shear modulus of GFRP bars limits their contribution to the dowel action. Based on this concept, Tureyen et al. (2003) developed a physical model for calculating the concrete contribution to the shear strength of GFRP-RC beams (Tureyen et al., 2003). The model considered a cracked section rather than a section between two cracks, as in the case of ACI 318-19 shear equations. The bond between two cracks in steel-RC allows a change in reinforcement stress distribution, leading to horizontal and vertical shear stress development above the flexural reinforcement. However, reinforcement stress does not change across the crack, eliminating the horizontal and vertical shear stresses in the web below the neutral axis. Therefore, concrete contribution below the neutral axis was neglected. The model proposed by Tureyen and Frosh for one-way shear strength is provided below as Eq. (8):

$$V_c = 0.42\sqrt{f'_c}bc, \tag{8}$$

where b = member width, mm; c = k_{cr} x d = cracked transformed section neutral axis depth, mm.

The axial stiffness of GFRP-reinforcement was considered through the ratio of the elastic cracked transformed neutral axis depth to the effective depth of the section, k_{cr}, which is a function of reinforcement ratio, ρ, and modular ratio, n. For a singly reinforced, rectangular cross-section without axial tension or compression, k_{cr}, may be determined using Eq. (9). However, its value may be determined based on strain compatibility and force equilibrium for non-rectangular cross-sections:

$$k_{cr,rect} = \sqrt{2\rho_f n_f + (\rho_f n_f)^2} - \rho_f n_f. \tag{9}$$

The reinforcement ratio, ρ, is calculated by dividing the longitudinal reinforcement area by the cross-section width and effective depth (i.e., A_f/bd). Meanwhile, the modular ratio, n_f, is achieved by dividing the elastic modulus of GFRP reinforcement by that of concrete (i.e., E_f/E_c).

Realizing the fact that the model suggested by Tureyen and Frosh would penalize lightly reinforced sections, a lower bound was proposed on the value of factor "k_{cr}" equal to 0.16 by Nanni et al. 2013 (Antonio et al., 2014). Both the equations proposed by Tureyen and Frosh, and Nanni et al. became part of ACI 440.11 Code as given in section 22.5.5.1 and provided below as Eqs (10) and (11):

$$V_c = 0.42\lambda_s k_{cr}\sqrt{f'_c}bd, \tag{10}$$

$$V_c = 0.066\lambda_s\sqrt{f'_c}bd, \tag{11}$$

where λ_s is size effect factor and its value be taken as provided in in ACI 440.11, Sect. 22.5.1.1 and provided below:

$$\lambda_s = \sqrt{\frac{2}{1+0.004}}. \tag{12}$$

Differently for GFRP-RC a hybrid-RC section has steel reinforcement in tension zone. The presence of steel bars changes the behavior of cracked RC section. A hybrid-section would offer more resistance to penetration of cracks due to higher stiffness of steel bars. The presence of steel bars will also limit the crack widths to smaller values compared to a GFRP-RC only section. Accordingly, aggregate interlock and dowel action may not be compromised. It is reasonable to assume that a similar amount of uncracked concrete would be available for a hybrid section as that of steel-RC. Therefore, it is a rational approach to estimate the shear strength provided by concrete in a hybrid-RC section using same model as that used for steel-RC. Consequently, it is proposed to calculate shear strength provided by concrete cross-section as per provisions of ACI 318-19 for steel-RC members. In the absence of axial force, shear strength provided by concrete can be calculated as per ACI 318-19, section 22.5.5.1a provided in Eq. (13). The contribution of FRP stirrups to shear strength should be calculated as per provision of ACI 440.11 Code (Table 1):

$$V_c = 0.17\lambda_s\sqrt{f'_c}bd. \tag{13}$$

2.5 Ductility Capacity

The ductility capacity of the cross-section considered in the present study was evaluated using the formulations outlined in the Italian Code (NTC, 2018, 2018). The use of this Code for the determination of capacity and demand in terms of ductility derives from the need to evaluate a local ductility and then move in future developments to global ductility assessments.

While Eurocode 8 (EC8) (Comité Européem de Normalisation, 2004), and the NTC 2018 (2018) provide specific formulations for the evaluation of ductility in curvature, it is worth noting that neither the ASCE standards nor the ACI codes offer similar formulations. Instead, ASCE standards, particularly ASCE 41-17, "Seismic Evaluation and Retrofit of Existing Buildings", and ACI codes such as ACI 318, "Building Code Requirements for Structural Concrete" provide detailed procedures for assessing the seismic capacity of structures, which may involve analyzing structural ductility (ACI Committee318-19, 2019; ASCE (41-17), 2017;). However, they do not provide specific formulations for evaluating ductility in curvature as found in European or Italian codes. Therefore, for the assessment of ductility in curvature in structures designed according to ASCE standards or ACI codes, it may be necessary to refer to specific resources within the technical literature or European and Italian standards for guidance. Therefore, it is proposed that to evaluate ductility and energy dissipation, Eurocode and Italian Codes may be referred until specific guidelines become available in North American Codes. Accordingly, in this study, above-mentioned Codes were referred for analysis of ductility and energy dissipation of a hybrid-RC cross-section.

The assessment of concrete confinement's significance in evaluating ductility is crucial for a comprehensive understanding of structural behavior, particularly in seismic environments. An experimental study scrutinized stress–strain models for normal and high-strength confined concrete, aimed to verify and compare the reliability of various literature models in replicating experimental results (Liborio et al., 2017). Cavaleri et al. underscored the indispensable role of concrete confinement in augmenting the seismic resilience of RC structures. They emphasized the significance of accurate estimations of concrete stress–strain constitutive laws in precisely calibrating nonlinear structural models and predicting safety conditions. Similarly, Chen et al., 2018 conducted a comparative analysis on the

Table 1 Existing and proposed equations

Quantity	Equations in the codes and proposed		
	GFRP-RC (ACI 440.11)	Steel-RC (ACI 318–19)	Hybrid-RC (proposed)
Strain	$C_{E^*}\varepsilon_{fu}$ [1]	0.005	0.005
Strength reduction factor for tension-controlled section	0.55	0.9	0.9
Minimum reinforcement area	$\frac{0.41\sqrt{f_c'}}{f_{fu}}bd$	$\frac{0.25\sqrt{f_c'}}{f_y}bd$	$\frac{0.25\sqrt{f_c'}}{f_y}bd$
Balanced reinforcement ratio	$\frac{0.85\beta_1 f_c'}{f_{fu}}\left(\frac{E_f\varepsilon_{cu}}{E_f\varepsilon_{cu}+f_{fu}}\right)$	$\frac{0.85\beta_1 f_c'}{f_y}\left(\frac{\varepsilon_{cu}}{\varepsilon_{cu}+\varepsilon_y}\right)$	$\frac{0.85\beta_1 f_c'}{f_y}\left(\frac{\varepsilon_{cu}}{\varepsilon_{cu}+\varepsilon_y}\right)$
Shear strength	$V_c + V_f$	$V_c + V_s$	$V_c + V_f$
Concrete contribution to shear strength	$\max(0.42\lambda_s k_{cr}\sqrt{f'_c}bd;$ $0.066\lambda_s\sqrt{f'_c}bd)$	$0.17\lambda_s\sqrt{f'_c}bd$	$0.17\lambda_s\sqrt{f'_c}bd$

[1] C_E is environmental reduction factor and ε_{fu}, guaranteed ultimate strain in GFRP bars

flexural performance of RC beams featuring external steel reinforcement confinement versus unconfined beams. In their conclusions, the authors highlighted that external steel confinement significantly improves flexural performance (Chen et al., 2018). Al-Etman et al., 2023 also delved into the flexural behavior of RC beams reinforced with FRP bars, employing both experimental and analytical methods to gauge the effectiveness of confinement in enhancing structural performance. The authors concluded that the use of GFRP stirrups can reduce cracking and enhance flexural ductility (Etman et al., 2023).

Ductility capacity in EC8 and NTC (2018) is a fundamental parameter that assesses the ability of a structure to undergo significant deformation beyond the elastic limit without experiencing collapse. This capacity is crucial, particularly in regions prone to seismic activity, where structures must withstand large displacements during earthquakes. In EC8, ductility capacity is quantified by comparing the post-peak strength curvature at 85% of the moment of resistance to the curvature at yield (Comité Européem de Normalisation, 2004). This comparison provides insights into the structural behavior under extreme loading conditions. The determination of ductility capacity according to the Italian Code closely aligns with the Eurocode approach, emphasizing the importance of evaluating structural behavior in terms of curvature (NTC, 2018, 2018). The equations provided in the NTC, 2018 offer a systematic framework for quantifying ductility capacity, considering both material properties and geometrical configurations. Ductility can be calculated as the ratio of the ultimate curvature to the curvature at yield, denoted as μ_ϕ as provided in Eq. (14):

$$\mu_\phi = \frac{\phi_u}{\phi_{yd}}, \tag{14}$$

where ϕ_u represents the ultimate curvature, which is the lowest of the last effective curvature of the section corresponding to the achievement of the limit deformation in the compressed concrete ε_{cu} and/or in the stretched steel ε_{su} and the curvature $\phi(M_{85\%})$ corresponding to the 15% reduction of the maximum resistance moment M_{Rd}:

$$\phi_u = \min[\phi(\varepsilon_{cu}, \varepsilon_{su}); \phi(M_{85\%})]. \tag{15}$$

ϕ_{yd} indicates the conventional curvature of the first section plasticization, defined by the relation in Eq. (16):

$$\phi_{yd} = \frac{M_{Rd}}{M_{yd'}}\phi'_{yd}. \tag{16}$$

As indicated in Eq. (16), ϕ_{yd} is determined by the ratio of M_{Rd} to $M_{yd'}$ multiplied by $\phi_{yd'}$, where $\phi_{yd'}$ is a reference curvature and $M_{yd'}$ the moment in correspondence of the reference curvature $\phi_{yd'}$.

Applying the equations and procedures delineated in NTC, 2018, the ductility capacities of the cross-section were determined. Specifically, the analysis focused on quantifying the ability of the hybrid-RC section to undergo significant deformation beyond the elastic limit without experiencing collapse. In the assessment of section ductility, emphasis is placed on concrete confinement as per the NTC, 2018 regulations, typically achieved through closed stirrups (or ties in columns). Confinement allows concrete to endure higher stresses and deformations compared to unconfined concrete, while other mechanical properties remain relatively unchanged.

The model outlined in Section §4.1.2.1.2.1 of the NTC, 2018 was employed in this study as provided in Fig 1.

ε_{c2} and ε_{cu} represent the concrete strain at the elastic limit and ultimate strain, respectively, for unconfined

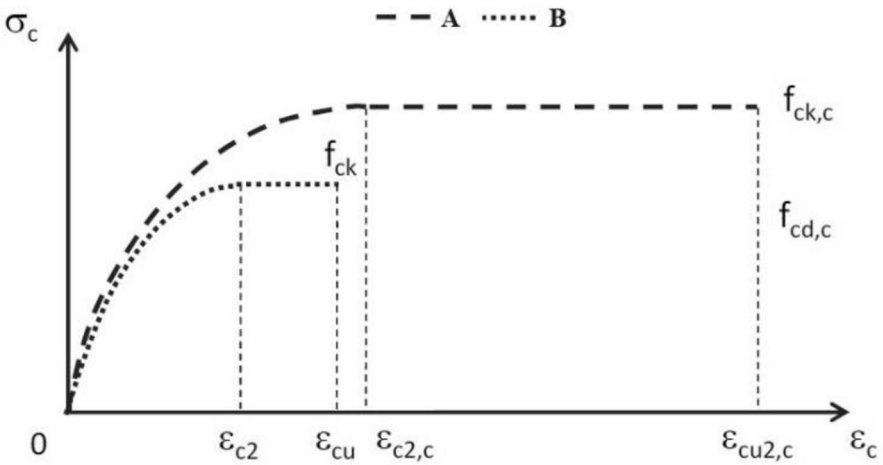

Fig. 1 Compressive behavior of concrete: **A** confined and **B** unconfined

concrete, while $\varepsilon_{c2,c}$ and $\varepsilon_{cu,c}$ for confined concrete. The figure shows a significant increase in the deformation and strength of confined concrete. The standard recommends adopting characteristic strength values unless specific conditions, such as verifying the strength and ductility of existing structures, dictate otherwise.

The strength and deformation capacity of confined concrete were evaluated following §4.1.2.1.2.1 of the NTC, 2018. The confinement pressure was calculated using Eq. (17):

$$\sigma_2 = \alpha\sigma_l. \tag{17}$$

Here, α denotes the confinement efficiency coefficient, which depends on factors like the quantity, arrangement, and spacing of transverse reinforcements, as well as the number of restrained longitudinal bars:

$$\sigma_l = \sqrt{\sigma_{l,x} + \sigma_{l,y}}. \tag{18}$$

σ_l represents the confinement pressure exerted by transverse reinforcement, with $\sigma_{l,x}$ and $\sigma_{l,y}$ can be calculated as per Eqs. (19) and (20):

$$\sigma_{l,x} = \frac{A_{st,x} f_{yk,st}}{b_y s}, \tag{19}$$

$$\sigma_{l,y} = \frac{A_{st,y} f_{yk,st}}{b_x s}, \tag{20}$$

where $A_{st,x}$ denotes the transverse reinforcement cross-sectional area; b_x indicates the width of the confined core in the same direction, with reference to the midline of the stirrups, while s and $f_{yk,st}$ represent the spacing and yield stress of transverse reinforcement, respectively. Similar definitions apply for the y-direction.

The ultimate strain of confined concrete, $\varepsilon_{cu,c}$, is determined by the following parabola–rectangle relationship (for concrete classes equal to or less than C50/60):

$$\varepsilon_{cu,c} = 0.0035 + 0.2\frac{\sigma_2}{f_{ck}}. \tag{21}$$

f_{ck} represents the characteristic value of compressive cylindrical strength of the material.

2.6 Energy Dissipation

In addition to assessing the ductility of RC elements, another critical aspect in structural engineering is the evaluation of their energy dissipation capacity. Energy dissipation refers to the ability of a structure to absorb and dissipate energy during dynamic loading events, such as earthquakes or wind gusts, thereby reducing the potential for damage or collapse. In reinforced concrete RC elements, energy dissipation mechanisms can include yielding of reinforcing steel, concrete cracking, and hysteretic damping effects. This section explores various methods and considerations for evaluating the energy dissipation capacity of RC elements.

In the context of developing advanced seismic analysis and design methodologies, several studies in the literature have addressed the challenge of accurately estimating the hysteretic behavior of RC elements, characterized by strength, deformability, and energy dissipation capacity. Park and Hong performed nonlinear finite element analysis to investigate the behavioral characteristics of flexure-dominated RC members under cyclic loading (Park & Hong-Gun, 2013). Based on the results, a simplified method was developed to estimate the energy dissipation capacity of such members, validated through comparisons with existing experiments on beams, columns, and structural walls. The proposed method carefully considers various design variables such as reinforcement ratio, arrangement, axial compression, and sectional shape. While the method does not fully capture the complexities of the overall hysteretic curve, it provides a valuable tool for nonlinear static and dynamic analysis in seismic design. The examined reference proposes the following formulation for energy dissipation:

$$E_D = e_D l_p, \tag{22}$$

$$e_D = 4R_B\rho f_y b h^2 \phi_u \left[(1-p)\left(\frac{1}{2}\frac{h_s}{h} - \frac{\varepsilon_y}{\phi_u h}\right) + p\left(\frac{1}{2} - \frac{\varepsilon_y}{\phi_u h}\right)^2\right], \tag{23}$$

where E_D is total energy dissipated by plastic hinge during cyclic loading, e_D is energy dissipated of a rectangular cross-section, R_B is reduction factor representing the Bauschinger effect, which is approximately set to 0.75, ρ is reinforcement ratio for total rebars, b, and h are width and depth of the rectangular cross-section, respectively, ϕ_u is maximum curvature, h_s is the distance between the rebar layers located at the boundaries, $p = \rho_w/\rho$ with ρ_w the ratio of uniformly distributed rebars and l_p is length of plastic hinge.

Understanding the plastic hinge length is essential for accurately predicting the structural response and ensuring the performance and safety of RC structures. Numerous formulations are present in the literature regarding the evaluation of its length, in this study the length of the plastic hinge was considered to be equal to the height of the hybrid section (h), following the recommendations outlined in the Building Seismic Safety Council (FEMA273/,1997, 1997).

3 Numerical Example

An illustrative design example of a HRC cross-section for a moment demand equal to 80 kN-m, and a shear equal to 70 kN is provided below. For this purpose, a rectangular cross-section was selected with the width (b) equal to 300 mm and depth (h) 440 mm. The concrete compressive strength (f'_c) used was taken equal to 40 MPa, and GFRP bars were compliant with material specifications ASTM D8505 (ASTM D8505, 2023). ASTM D8505 addresses both low elastic modulus bars currently specified by ACI 440.11 Code and high elastic modulus bars available in marketplace. In this study, high elastic modulus bars were selected as low elastic modulus bars are no longer used for construction projects. The mechanical properties of GFRP bars affecting design include guaranteed ultimate tensile strength, f_{fu}, corresponding ultimate strain ε_{fu}, modulus of elasticity E_f, and modular ratio n_f. A value of 1.20 for the bond coefficient, k_b, and 0.85 for the environmental reduction factor, C_E, are adopted as indicated in ACI 440.11-22 sections 24.3.2.3 and 20.2.2.3, respectively (ACI Committee440, 2022).

GFRP bars were placed at 38 mm from the concrete surface, whereas steel bars at 75 mm. The longitudinal GFRP reinforcement consisted of 2-M19 GFRP bars with a nominal diameter of 19.1 mm and a nominal area of 284 mm^2. Longitudinal steel bars had a diameter of 13 mm, with nominal area 129 mm^2. M13 GFRP stirrups were utilized for shear demand, whereas M8 steel stirrups were considered to hold steel bars in place. The steel bars had a yield strength equal to 420 MPa and were placed at a minimum practical distance to avoid corrosion from the surface of the concrete (i.e., 75 mm). The properties of reinforcement used in this study are provided in Table 2. The specific detailing of the reinforcement is out of scope of this study, readers are encouraged to consult Chapter 18 of ACI 318-19 for comprehensive guidance on reinforcement detailing for structures in seismic zones.

Ductility of the cross-section was calculated as per EC8 and NTC, 2018. Due to complex calculations involved in evaluating the ductility of entire structure, it was only calculated locally. Similarly, energy dissipation of the cross-section was calculated as per procedure presented by Park and Hong-Gun (2013) (Park & Hong-Gun, 2013).

3.1 Flexure Design

The cross-section was designed as per provisions of ACI 440.11, and ACI 318-19 in addition to the assumption mentioned in section 2 of this paper (ACI Committee318-19, 2019; ACI Committee440, 2022). Since two different types of reinforcement were used, therefore, two different effective depths (i.e., d_f: effective depth to GFRP reinforcement, and d_s: effective depth to steel reinforcement) were used in the analysis of cross-section. The nominal capacities provided by each reinforcement were added together and multiplied with an overall strength reduction factor equal to 0.9 as the strain in steel exceeded 0.005.

In the current design example, the effective depth (d_f) to the center of GFRP rebars was equal to 384 mm, whereas that for steel bars was equal to 345 mm. The minimum reinforcement ratio required as per Eq. (4) was equal to 0.0037, and for the moment demand was equal to 0.0038. Therefore, reinforcement ratio provided for the design of the cross-section was equal to 0.004. The provided reinforcement ratio was calculated by transforming GFRP bars to equivalent steel reinforcement (i.e., $\rho_{total} = (\rho_s + (\rho_f E_f / E_s))$.

The moment capacity provided by steel reinforcement was calculated using the steel reinforcement area in tension, yielding strength of steel (i.e., 420 MPa), and effective depth equal to the distance from extreme compression fiber to the centroid of steel bars (i.e., d_s). Similarly, the capacity supplemented by GFRP bars was calculated using GFRP reinforcement area, the stress in the bars, and effective depth measured from extreme compression fiber to the centroid of GFRP tension reinforcement (i.e., d_f). The flexural capacity provided by each type of reinforcement was added together as stated in ACI 440.1R-15 (2015) and multiplied with strength reduction factor (i.e., 0.9 for hybrid-RC). The design strength of the cross-section was equal to 90 kN-m, which exceeded the demand 80 kN-m. Fig. 2 shows the

Table 2 Properties of GFRP and steel rebars

Bar type	Nominal diameter (mm)	Cross-sectional area (mm^2)	Yield strength (MPa)	Ultimate tensile strength (MPa) Average	Modulus of elasticity (GPa)	Ultimate and yield strain (%)
GFRP	19.1	200.0	-	897.5	60.0	0.015
	12.7	129.0	-	962.0	60.0	0.016
Steel	12.7	129.0	420.0	-	200.0	0.002
	8.0	71.0	420.0	-	200.0	0.002

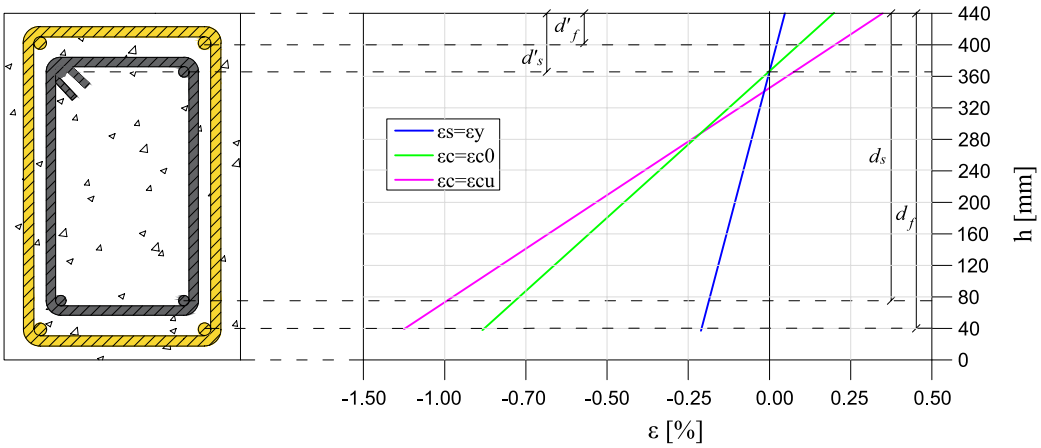

Fig. 2 Strain diagram of a hybrid-RC section at varying neutral axis depth

depth of neutral axis before cracking, at yielding of steel and failure. In Fig. 2, ε_s, is strain in steel bars in tension, ε_y, is yielding strain in steel bars, ε_c, is strain in concrete on compression side of cross-section, ε_{co}, is the elastic limit of concrete taken equal to 0.002, and ε_{cu}, is ultimate strain in concrete taken equal to 0.003.

The strain at failure in FRP bars was equal to 0.0059, and in steel bars was equal to 0.0051. It should be noted that strain in steel bars (i.e., 0.0051) indicates that steel bars entered into the plastic zone and that the cross-section dissipates energy. The contribution of reinforcement on the compression side of the cross-section should be considered based on the position of neutral axis depth. In the current design example, the neutral axis at failure falls below the location of reinforcement on compression side, which contributes to compressive force. However, in hybrid-section design the position of neutral axis shifts quickly depending on the diameter of GFRP and steel bars. Hence particular attention may be given towards the contribution of reinforcement on the compression side of section. Fig 3 presents the reinforcement details used in the cross-section design.

The cross-section capacity was greater than twice the cracking moment of the cross-section. For example, the cracking moment calculated using cross-section dimensions and material properties was equal to 38 kN-m, whereas capacity of the cross-section was 90 kN-m. This satisfies the purpose of code specifications for minimum reinforcement requirements.

3.2 Shear Design

The nominal shear strength of the hybrid section was calculated as discussed in section 2.4, Eq. (7). Shear strength provided by concrete cross-section V_c was calculated as per provisions of ACI 318-19 provided as Eq. (13) in this paper. The size effect factor was also considered in the design, since cross-section depth exceeds 250 mm. Shear strength provided by the GFRP reinforcement may be calculated as given in the ACI 440.11 Code section 22.5.8.5.3 provided below:

$$V_f = A_{fv} f_{ft} \frac{d}{s}, \tag{24}$$

where A_{fv}, is the area of shear reinforcement calculated as given in the Code Commentary equation R22.5.8.5 given below:

$$\frac{A_{fv}}{s} = \frac{V_u - \Phi V_c}{\Phi f_{ft} d}, \tag{25}$$

where f_{ft}, is the permissible stress in the GFRP shear reinforcement. The design tensile strength of GFRP transverse reinforcement is controlled by the strength of the bent portion of the bar and by a strain limit of 0.005 as given by Code section 20.2.2.6.

$$f_{ft} \le \left(f_{fb}, 0.005 E_f\right), \tag{26}$$

where $f_{fb} = C_E f_{fb}^{*}$= design tensile strength of the bent portion of GFRP reinforcement.

$F_{fb}{}^{*}$ is the guaranteed ultimate tensile strength of bent portion of bar. Its minimum value is taken as specified in ASTM D8505 by dividing ultimate guaranteed tensile force of bent portion of the bar by nominal cross-section area of the bar.

Maximum spacing of stirrups is still governed by ACI 440.11 code as it is based on the shear capacity of GFRP stirrups. Therefore, in this study maximum spacing of GFRP stirrups was taken as provided in ACI 440.11. Maximum spacing between legs of shear reinforcement was calculated as the least of maximum spacing

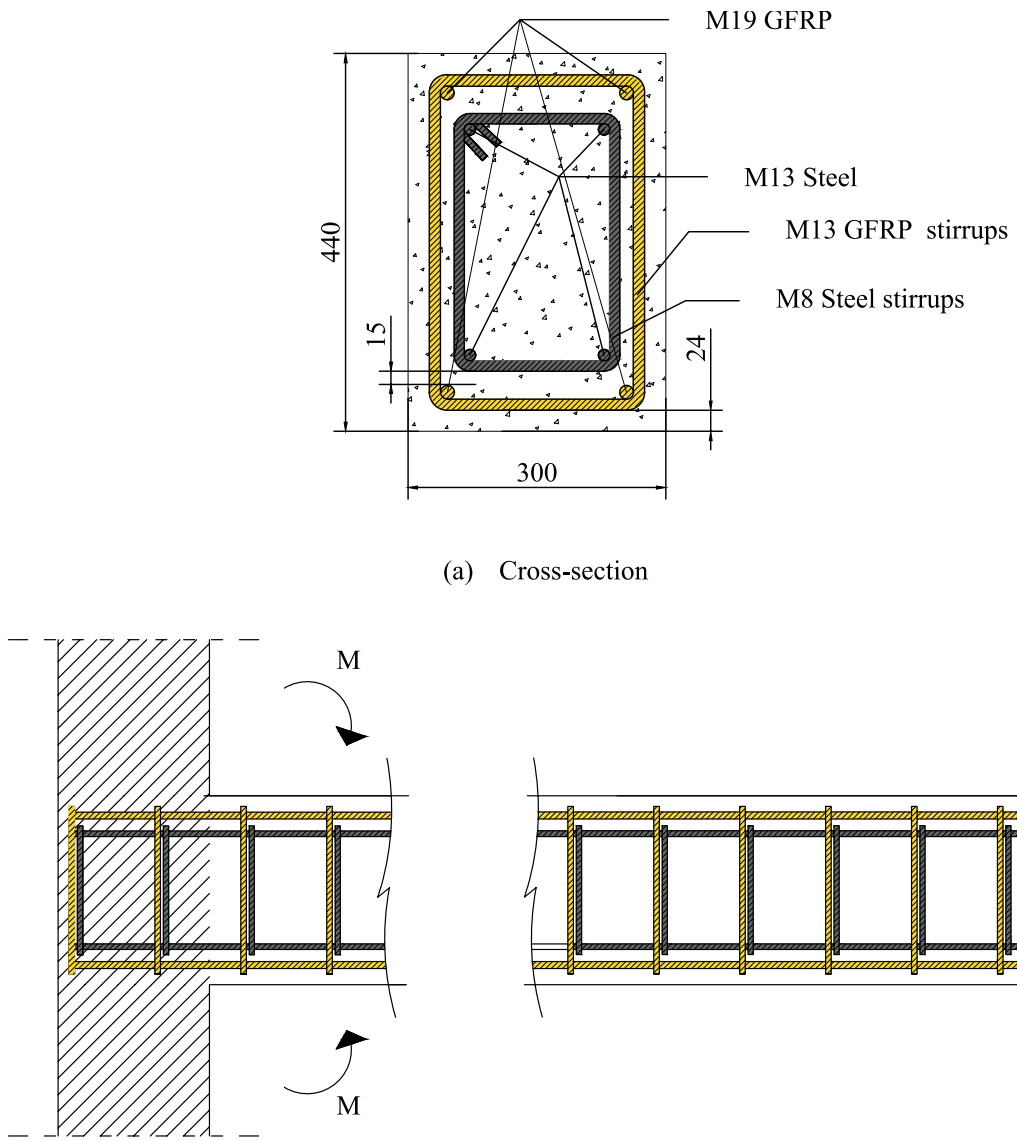

(a) Cross-section

(b) Longitudinal section

Fig. 3 Reinforcement details (details are not provided for anchorage of longitudinal bars)

limitations given by the Code and its Commentary in sections R22.5.10.5, 9.6.3.4 and 9.7.6.2.2.

$$s_{max} = min\begin{cases} \frac{A_{fv}\Phi f_{ft} d}{V_u - \Phi V_c} R22.5.10.5 \\ \frac{A_{fv} f_{ft}}{0.062\sqrt{fc}b} 9.6.3.4a \\ \frac{A_{fv} f_{ft}}{0.35b} 9.6.3.4b \\ min(\frac{d}{2}, 610mm) 9.7.6.2.2 \end{cases} \quad (27)$$

The contribution of concrete cross-section towards shear capacity is lower if calculated as per ACI 440.11. Together with a 40% reduction in the strength at the bend of GFRP transverse reinforcement, it significantly affects the shear design of GFRP-RC compared with steel-RC. However, in the design of hybrid-RC sections, V_c can be calculated as per provisions of ACI 318-19, i.e., as in the case of steel-RC sections. Therefore, V_c calculated was 125% more compared to one calculated as per provisions of ACI 440.11, i.e., in the case of GFRP-RC sections. For example, V_c calculated as per ACI 440.11 section 22.5.5.1 was equal to 43 kN, compared to 108 kN as per section 22.5.5.1 of ACI 318-19. The contribution of GFRP stirrups to shear strength would be lower compared to the one of steel stirrups due to limits imposed on the maximum contribution of GFRP stirrups. For example,

the guaranteed tensile strength of M13 bars is 770 Mpa, however, their maximum contribution cannot be greater than $0.005E_f$ (i.e., 225 Mpa). This limit is imposed to avoid loss of aggregate interlock. Therefore, the combined shear strength of concrete section and GFRP stirrups in a hybrid-RC would be lower than steel-RC but greater than GFRP-RC. In this design example, shear capacity provided by concrete cross-section was equal to 108 kN which is greater than demand 70 kN. However, stirrups should still be provided at a maximum distance allowed by code in section 9.7.6.6.2 as provided in Eqs. (27–30). Therefore, in the current design example GFRP stirrups were provided at 190 mm center-to-center.

It has been reported in the literature that the shear failure in GFRP-RC members occur by opening of stirrup legs. Therefore, it is recommended to provide stirrups with two overlaps as shown below in Fig. 4.

3.3 Ductility Capacity of the Cross-Section

The ductility of the section under study in terms of curvature was assessed by considering both the contribution of confined and non-confined concrete with reference to Eq. (14). The assessment concerned the examination of how the presence of confinement, provided by both steel and GFRP brackets in the section under consideration, affects the overall ductility. By integrating the specific confinement effects of the section under consideration, the analysis aimed to provide a more accurate representation of its performance, particularly in seismic scenarios where ductility is of paramount importance.

The formulations and constitutive relationships presented in section 2.5 refer to concrete confined by steel stirrups. In the case under consideration, there are both steel stirrups on the inner core of the section and GFRP stirrups on the outside. Based on the experimental results reported in Dong et al., 2018 and pending further studies aimed at assessing the confinement of GFRP stirrups on concrete, the concrete confinement in this case was evaluated by adapting the formulations provided in the NTC, 2018 for steel stirrups to GFRP stirrups (Dong et al., 2018). Therefore, the constitutive relationship of C40/45 concrete used for the ductility assessment of the section under study is depicted in Fig 5.

The ultimate curvature of the section under study was assessed by considering the attainment of ultimate strain of confined concrete (assumed at the level of longitudinal GFRP bars). In Fig. 6, ε_s, is strain in steel bars in tension, ε_y, is yielding strain in steel bars, ε_c, is strain in concrete on compression side of cross-section, ε_{co}, is the elastic limit of concrete taken equal to 0.002, ε_{cu}, is ultimate strain in concrete taken equal to 0.0035 (Comité Européem de Normalisation, 2004; NTC, 2018, 2018), and $\varepsilon_{cu,c}$ is the ultimate strain in confined concrete.

In Fig. 6, the assessment of the neutral axis and, consequently, the curvature of the section (as depicted by the slope of the stress–strain diagram) is presented for four key conditions: 1) $\varepsilon_s = \varepsilon_{sy}$ upon reaching the yield strain (ε_{sy}) in the tensile steel bars; 2) $\varepsilon_c = \varepsilon_{c0}$ at the attainment of the elastic limit strain (ε_{c0}) of the concrete at the compressed end; 3) $\varepsilon_c = \varepsilon_{cu}$ upon reaching the ultimate strain (ε_{cu}) of the concrete at the compressed end; 4) $\varepsilon_c = \varepsilon_{cu,c}$ upon reaching the ultimate strain ($\varepsilon_{cu,c}$) of the confined concrete at the region confined by GFRP bars, with the contribution of the upper concrete neglected to exceed the ultimate strain value ε_{cu}. The figure illustrates a notable variation in the depth of the neutral axis and consequently the curvature of the section, particularly considering the confinement of the concrete. The results obtained from the assessment of the section under study are presented in Table 3.

Table 3 summarizes the ductility capacities of the section, highlighting the contributions of confinement and unconfined concrete. It becomes evident from the results that the presence of concrete confinement plays a crucial

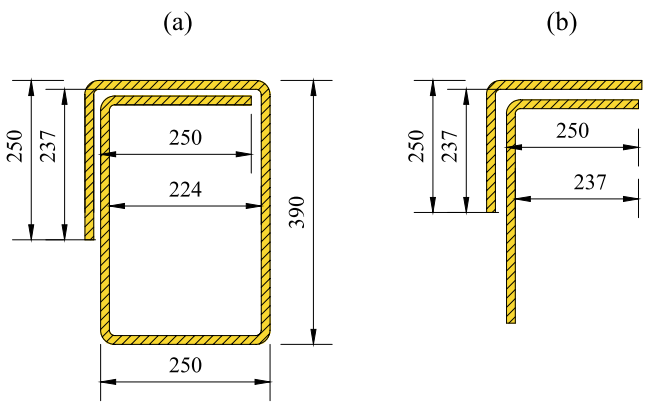

Fig. 4 Reinforcement details: **a** GFRP stirrup, **b** stirrups overlaps

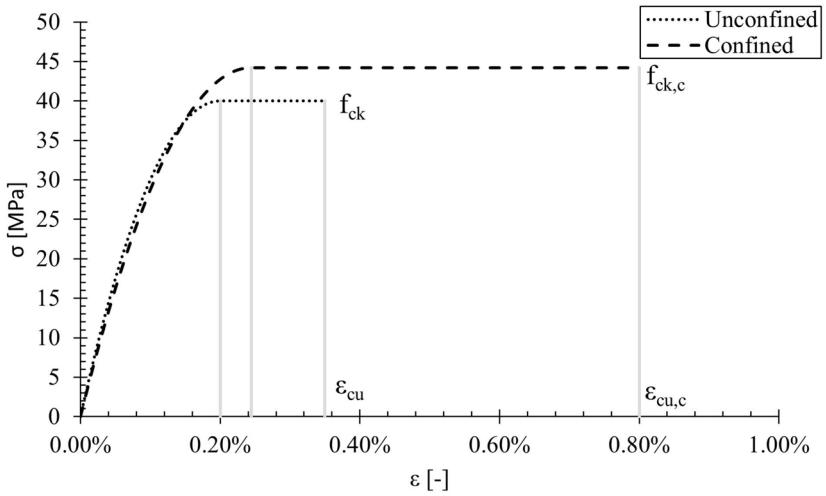

Fig. 5 Concrete C40/45 compressive behavior

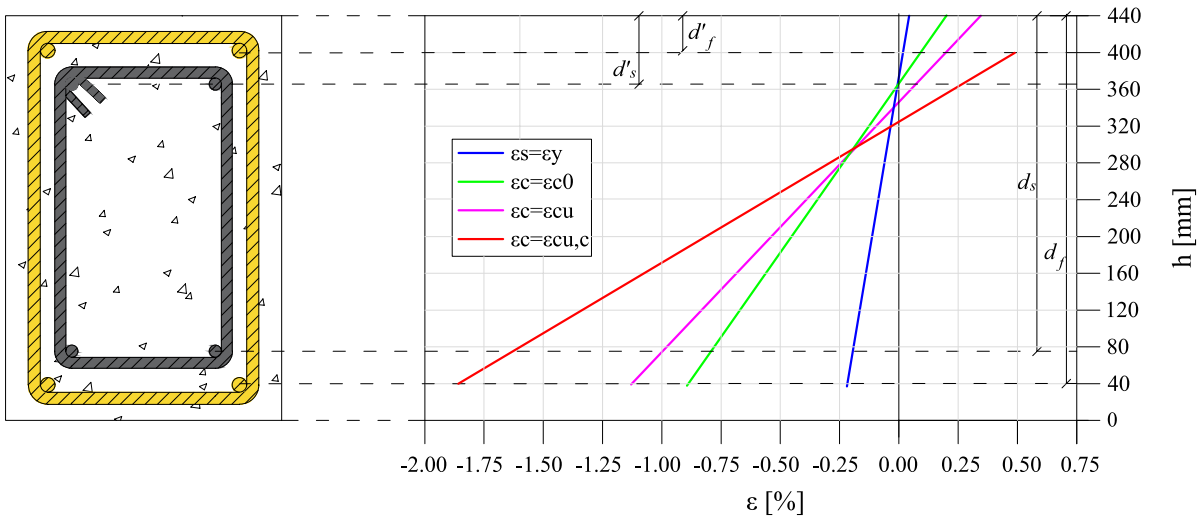

Fig. 6 Strain diagram of a hybrid-RC section with confined concrete

Table 3 Ductility capacity

Section	f'_c (MPa)	ε_{cu}	μ_ϕ
Unconfined	40	0.0035	4.8
Confined	44	0.0077	16.8

role in enhancing the section's ductility, as shown by condition 4 $\left(\varepsilon_c = \varepsilon_{cu,c}\right)$ in Fig. 6; however, such a condition is governed by the ultimate strain of the GFRP, partially limiting the concrete confinement effect to ensure compatibility of deformations. By effectively restraining lateral expansion and increasing compressive strength, confinement significantly improves the section's ability to deform without experiencing failure.

The ductility capacity of the cross-section (i.e., 16.8), assessed considering confinement, aligns well with the curvature demand of SDC D as identified by ASCE 7-16 (2016). The ductility demand was evaluated in accordance with Eurocode 8, §5.2.3.4.3, using Equation (31):

$$\mu_{\chi,d} = \begin{cases} 2q_0 - 1 \; if \; T_1 \geq T_C \\ 1 + 2(q_0 - 1)\frac{T_C}{T_1} \; if \; T_1 < T_C \end{cases}, \tag{28}$$

where q_0 is the basic behavior factor, T_1 is the fundamental period of the structure, and T_C is the upper limit of the constant spectral acceleration branch. The behavior factor q_0 was determined by correlating it with the equivalent factor in ASCE 7–16, defined as:

$$q_0 = \frac{R}{I_e}. \tag{29}$$

In this equation, R is the response modification coefficient, taken as 8 according to Table 12.2-1 (ASCE7-16, 2016) e I_e is the importance factor, assumed as 1.25 for seismic risk category III as specified in Table 1.5–2. (ASCE7-16, 2016). These values are consistent with SDC D requirements. The ductility demand, assessed across a range of possible fundamental periods T_1 and different peak ground acceleration values characteristic of SDC D, resulted in values between 13 and 22.

3.4 Energy Dissipation of the Cross-Section

The assessment of energy dissipation capacity for the section was conducted in accordance with the formulations outlined in Section 2.6. This methodical approach ensures a comprehensive evaluation of the section's ability to dissipate energy, crucial for its performance under dynamic loading conditions such as seismic events. The parameters considered for evaluating the energy dissipation of the section and the results obtained are summarized in Table 4.

This choice aligns with established guidelines for seismic rehabilitation and reinforces the importance of considering plastic hinge length in structural analysis and design. By adopting this approach, consistency with industry standards is ensured, enhancing the reliability of the assessment of energy dissipation capacity. Table 4 provides a comprehensive overview of the parameters used in evaluating the energy dissipation of the hybrid section, including the dimensions of the section, reinforcement ratio, and other key variables. The results obtained from these evaluations offer valuable insights into the energy dissipation characteristics of the hybrid-RC sections under consideration. Similarly to the assessment of ductility, the influence of concrete confinement can be appreciated. Concrete confinement plays a crucial role in enhancing the energy dissipation capacity of RC elements.

4 Conclusions and Recommendations

In this study design and analysis of a hybrid-RC section was carried out to develop an understanding about design, ductility and energy dissipation of cross-sections designed with hybrid GFRP-steel reinforcement. The cross-section was designed with M19-GFRP bars placed at 38 mm and M13 steel bars at 75 mm from concrete cross-section surface. The concrete strength was taken equal to 40 MPa. Based on the analysis and design the following conclusions were drawn:

- It is possible to design a hybrid-RC cross-section using GFRP and steel bars. However, care should be taken to properly select the reinforcement configuration. A proper selection of reinforcement area is necessary to make sure that strain in steel bars at failure exceeds 0.005 prior to GFRP rupture.
- The minimum reinforcement area required to have the ultimate moment capacity greater than the cracking moment may be calculated as per provisions of ACI 318–19.
- Assuming a strain in steel bars greater than 0.005, a strength reduction factor equal to 0.9 may be used when calculating the design strength of a hybrid-RC section.
- The shear capacity of a hybrid-RC section may be calculated as sum of the strength contributions of concrete and GFRP stirrups. Due to the presence of the longitudinal steel bars, the concrete contribution to shear strength may be calculated as per provisions of ACI 318–19. The contribution of steel stirrups to the shear strength may be conservatively ignored.
- To calculate ductility and energy dissipation, the effect of confinement provided by GFRP stirrups is taken equal to that of steel stirrups. However, an experimental study is warranted to develop confinement factors similar to the ones in Eurocode and Italian code.
- Using 2-M19 GFRP and 2-M13 steel bars, the ductility of the cross-section was calculated equal to 16.8 and energy dissipation 4.7 kN-m, which make this hybrid-RC section acceptable in SDC D.

Table 4 Evaluation capacity of energy dissipated

Designation	ρ (-)	b (mm)	h (mm)	h_s (mm)	ϕ_u (1/m)	p (-)	l_p (mm)	e_D (kN)	E_D (kN-m)
Unconfined	0.002	300	440	483	0.000082	0.5	440	2.2	1.0
Confined					0.00026			3.2	1.7

The present paper contributes in terms of design and assessment criteria, reviewing, comparing, and extending current codes. Therefore, this study can be viewed as an analytical/design proposal awaiting confirmation and refinement based on forthcoming experimental results. Further studies will experimentally assess the hybrid members, possibly corroborating the findings of the study.

Acknowledgements
The authors gratefully acknowledge the financial support provided by the National Science Foundation IU-CRC Center for Integration of Composites into Infrastructure (CICI) under grant #1916342, Program of international exchanges between the University of Naples Federico II and foreign research institutes for short-term mobility of teachers, scholars, and researchers, issued with DR/2022/2084 del 19/05/2022, and Superior Council of Public Works in the framework of the national ReLUIS project n.31 dated 23 June 2021.

Author contributions
Zahid Hussain: conceptualization, writing—original draft, methodology, investigation, analysis. Federico Tuaozzo: conceptualization, writing—original draft, methodology, investigation, analysis. Gennaro Magliulo: conceptualization, methodology, analysis, review. Antonio Nanni: conceptualization, methodology, analysis, review.

Data availability
All the data used appear in the manuscript.

Declarations

Ethics approval and consent to participate
Not applicable.

Consent for publication
All authors have read and approved the final manuscript. We confirm that this manuscript has not been published elsewhere and is not under consideration by another journal. We consent to the publication of this manuscript in the *International Journal of Concrete Structures and Materials*.

Competing interests
The authors declare that they have no known competing financial interests or personal relationships that could have appeared to influence the work reported in this paper.

Received: 3 August 2024 Accepted: 11 December 2024
Published online: 09 April 2025

References

ACI 440.1R-15. (2015). *Guide for the Design and Construction of Structural Concrete Reinforced with Fiber-Reinforced Polymer (FRP) Bars*. Farmington Hills, MI. ISBN: 978-1-942727-10-1. Retrieved from https://www.concrete.org/Portals/0/Files/PDF/Previews//440_1R_15.pdf.

ACI Committee 318-19. (2019). Building Code Requirements for Structural Concrete (ACI 318-19) and Commentary (ACI 318R-19). Farmington Hills MI. https://doi.org/10.14359/51716937

ACI Committee 440. (2022). *Building code requirements for structural concrete reinforced with glass fiber-reinforced polymer (GFRP) bars: code and commentary* (Vol. 1). Retrieved from https://www.concrete.org/Portals/0/Files/PDF/Previews//440.11-22_Preview.pdf.

Antonio, N., Antonio, D. L., & Hany Jawaheri, Z. (2014). *FRP Reinforced Concrete Structures – Theory, Design and Practice* (1st ed.). CRC Press. https://doi.org/10.1201/b16669

ASCE 7-16. (2016). *Minimum Design Loads and Associated Criteria for Buildings and other Structures*. https://doi.org/10.1061/9780784414248

ASCE (41–17). (2017). *Seismic evaluation and retrofit of existing buildings*. 9780784414859

ASTM D7957/D7957M-22. (2022). Standard Specifications for Solid Round Glass Fiber Reinforced Polymer Bars for Concrete Reinforcement. West Conshocken, OA. https://doi.org/10.1520/D7957_D7957M-22

ASTM D8505. (2023). Standard specification for basalt and glass fiber reinforced polymer (FRP) bars for concrete reinforcement. Farmington Hills, MI. https://doi.org/10.1520/D8505_D8505M-23

Benmokrane, B., & Masmoudi, R. (1995). Flexural response of concrete beams reinforced with FRP reinforcing bars. *ACI Structural Journal*. https://doi.org/10.14359/9839

Chen, W., Pham, T. M., Sichembe, H., Chen, L., & Hao, H. (2018). Experimental study of flexural behaviur of RC beams strengthened by longitudinal and U-shaped basalt FRP sheet. *Composites Part b: Engineering, 134*, 114–126. https://doi.org/10.1016/j.compositesb.2017.09.053

Comité Européem de Normalisation. (2004). *Eurocode 8: Design of Structures for Earthquake Resistance (in Italian)*. https://doi.org/10.1680/cien.2001.144.6.55

Deng, Z., Gao, L., & Wang, X. (2018). Glass fiber-reinforced polymer-reinforced rectangular concrete columns under simulated seismic loads. *Journal of the Brazilian Society of Mechanical Sciences and Engineering, 40*, 1–12. https://doi.org/10.1007/S40430-018-1041-8

Dong, H.-L., Wang, D., Wang, Z., & Sun, Y. (2018). Axial compressive behavior of square concrete columns reinforced with innovative closed-type winding GFRP stirrups. *Composite Structures, 192*, 115–125. https://doi.org/10.1016/j.compstruct.2018.02.092

Etman, E. E., Mahmoud, M. H., Hassan, A., & Mowafy, M. H. (2023). Flexural behaviour of concrete beams reinforced with steel-FRP composite bars. *Structures, 50*, 1147–1163. https://doi.org/10.1016/j.istruc.2023.02.098

FEMA 273/1997. (1997). *NEHRP Guidelines for the Seismic Rehabilitation of Buildings*. Washington. https://courses.washington.edu/cee518/fema273.pdf.

Japan Society of Civil Engineers. (1997). *Recommendation for Design and Construction of Concrete Structures Using Continuous Fiber Reinforcing Materials*. Tokyo. https://www.jsce.or.jp/committee/concrete/e/web/pdf/31-1.pdf.

Joint ACI-ASCE Committee 445. (1998). Recent approaches to shear design of structural concrete. *Journal of Structural Engineering*, 1375–1417.

Liborio, C., Fabio Di, T., Marco Filippo, F., & Luigi, D. (2017). Stress-strain models for normal and high strength confined concrete: test and comparison of literature models reliability in reproducing experimental results. *International Journal of Earthquake Engineering*. https://iris.polito.it/handle/11583/2687411

NTC 2018. (2018). *Norme Tecniche per le Costruzioni (in Italian)*. Retrieved from https://biblus.acca.it/download/norme-tecniche-per-lec-costruzioni-2018-ntc-2018--pdf/

Park, T.-S.E., & Hong-Gun. (2013). Evaluation of shear deformation and energy dissipation of reinforced concrete members subjected to cyclic loading. *ACI Structural Journal, 110*(5), 845–854. https://doi.org/10.14359/51685837

Prajapati, G. N., Farghaly, A. S., & Benmokrane, B. (2023). Behavior of glass fiber-reinforced polymer-reinforced concrete columns subjected to simulated seismic load. *ACI Structural Journal, 120*(1), 3–16. https://doi.org/10.14359/51737228

Tavassoli, A., Liu, J., & Sheikh, S. (2015). Glass fiber-reinforced polymer-reinforced circular columns under simulated seismic loads. *ACI Structural Journal*. https://doi.org/10.14359/51687227

Tureyen, A. K., & Frosh, J. R. (2003). Concrete shear strength; another perspective. *ACI Structural Journal, 100*(5), 609–615. https://doi.org/10.14359/12802

Publisher's Note

Zahid Hussain is a PhD candidate in the Civil and Architectural Engineering Department at the University of Miami. He is a student member of ACI Committee 440, Fiber Reinforced Polymer

Reinforcement. His research interests include sustainable materials, computational methods, design, and behavior of reinforced concrete structures.

Federico Tuozzo is a PhD student in Structural, Geotechnical Engineering, and Seismic Risk Engineering at the Department of Structures for Engineering and Architecture at the University of Naples Federico II. His research includes the structural design and assessment of reinforced concrete structures in seismic zones, with a particular focus on viaducts, nonlinear dynamic analysis, and detailed finite element modeling.

Gennaro Magliulo is Associate Professor of Structural Engineering at the Department of Structures for Engineering and Architecture University of Naples Federico II. He is qualified for Italian Full Professorship of "Structural Design" and is affiliate researcher at the Construction Technologies Institute of the National Research Council. He is member of the board of ACI Italy Chapter and of "Seismic Performance of Non-structural Element" association.

Antonio Nanni is an Inaugural Senior Scholar, Professor, and Chair of the Department of Civil and Architectural Engineering at the University of Miami. He is a member of ACI Committee 549, Thin Reinforced Cementitious Products and Ferrocement, and ACI Committee 440, Fiber Reinforced Polymer Reinforcement.